

SalsaNext: Fast Semantic Segmentation of LiDAR Point Clouds for Autonomous Driving

Tiago Cortinhal¹, George Tzelepis² and Eren Erdal Aksoy^{1,2}

Abstract—In this paper, we introduce *SalsaNext* for the semantic segmentation of a full 3D LiDAR point cloud in real-time. *SalsaNext* is the next version of *SalsaNet* [1] which has an encoder-decoder architecture where the encoder unit has a set of ResNet blocks and the decoder part combines upsampled features from the residual blocks. In contrast to *SalsaNet*, we have an additional layer in the encoder and decoder, introduce the context module, switch from stride convolution to average pooling and also apply central dropout treatment. To directly optimize the Jaccard index, we further combine the weighted cross entropy loss with *Lovász-Softmax* loss [2]. We provide a thorough quantitative evaluation on the Semantic-KITTI dataset [3], which demonstrates that the proposed *SalsaNext* outperforms other state-of-the-art semantic segmentation networks in terms of accuracy and computation time. We also release our source code <https://github.com/TiagoCortinhal/SalsaNext>.

I. INTRODUCTION

Scene understanding is an essential prerequisite for autonomous vehicles. Semantic segmentation helps gaining a rich understanding of the scene by predicting a meaningful class label for each individual sensory data point. Achieving such a fine-grained semantic prediction in real-time accelerates reaching the full autonomy to a great extent.

Advanced deep neural networks have recently had a quantum jump in generating accurate and reliable semantic segmentation with real-time performance. Most of these approaches, however, rely on the camera images [4], [5], whereas relatively fewer contributions have discussed the semantic segmentation of 3D LiDAR data [6], [7]. The main reason is that unlike camera images, LiDAR point clouds are relatively sparse, unstructured, and have non-uniform sampling although LiDAR scanners have wider field of view and return more accurate distance measurements.

As comprehensively described in [8], there exist two mainstream deep learning approaches addressing the semantic segmentation of 3D LiDAR data only: point-wise and projection-based neural networks (see Fig. 1). The former approaches operate directly on the raw 3D points without requiring any pre-processing step, whereas the latter project the point cloud into various formats such as 2D image view or high-dimensional volumetric representation. As illustrated in Fig. 1, there is a clear split between these two approaches in terms of accuracy, runtime and memory consumption.

The research leading to these results has received funding from the Vinnova FFI project SHARPEN, under grant agreement no. 2018-05001.

¹Halmstad University, School of Information Technology, Center for Applied Intelligent Systems Research, Halmstad, Sweden.

²Volvo Technology AB, Volvo Group Trucks Technology, Vehicle Automation, Gothenburg, Sweden.

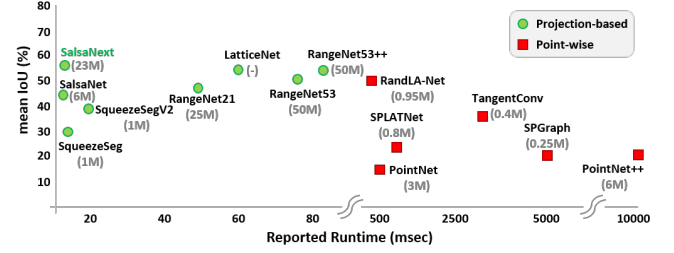


Fig. 1. Mean IoU versus runtime plot for the state-of-the-art 3D point cloud semantic segmentation networks. Inside parentheses are given the total number of network parameters in Millions. All deep networks visualized here use only 3D LiDAR point cloud data as input. The results are computed on the Semantic-KITTI dataset [3] and most of them are reported in [7]. Note that only the published methods are considered.

For instance, projection-based approaches (shown in green circles in Fig. 1) achieve the state-of-the-art accuracy while running significantly faster. Although point-wise networks (red squares) have slightly less number of parameters, they cannot efficiently scale up to large point sets due to the limited processing capacity, thus, they take a longer runtime.

In this work, we introduce a new neural network to perform semantic segmentation of a full 3D LiDAR point cloud in real-time. Our proposed network is build upon the *SalsaNet* model [1], hence, named *SalsaNext*. The *SalsaNet* model has an encoder-decoder skeleton where the encoder unit consists of a series of ResNet blocks and the decoder part upsamples and fuses features extracted in the residual blocks. The here proposed *SalsaNext* incorporates the following improvements over the *SalsaNet* version:

- To process the full 360° LiDAR scan, the network depth was increased by inserting additional layers in the encoder and decoder units.
- To capture the global context information, a new context module was introduced before the encoder unit.
- To boost the roles of very basic features (e.g. edges and curves) in the segmentation process, the dropout treatment was altered by omitting the first and last network layers in the dropout process.
- To have a lighter model, average pooling was employed instead of having stride convolutions in the encoder.
- To enhance the segmentation accuracy by optimizing the mean intersection-over-union score, i.e. the Jaccard index, the weighted cross entropy loss in *SalsaNet* was combined with the *Lovász-Softmax* loss [2].

All these contributions form the here introduced *SalsaNext* model which has a significantly better segmentation perfor-

mance. The input of *SalsaNext* is the rasterized image of the full LiDAR scan, where each image channel stores position, depth, and intensity cues in the panoramic view format. The final network output is the point-wise classification scores.

Quantitative and qualitative experiments on the Semantic-KITTI dataset [3] show that the proposed *SalsaNext* significantly outperforms other state-of-the-art networks in terms of pixel-wise segmentation accuracy while having much less parameters and thus requiring less computation time.

Note that we also release our source code and trained model to encourage further research on the subject <https://github.com/TiagoCortinhal/SalsaNext>.

II. RELATED WORK

Recently, great progress has been achieved in semantic segmentation of 3D LiDAR point clouds using deep neural networks [1], [6], [7], [9], [10]. The core distinction between these advanced methods lies not only in the network design but also in the representation of the point cloud data.

Fully convolutional networks [11], encoder-decoder structures [12], and multi-branch models [5], among others, are the mainstream network architectures used for semantic segmentation. Each network type has a unique way of encoding features at various levels, which are then fused to recover the spatial information. Our proposed *SalsaNext* follows the encoder-decoder design as it showed promising performance in most state-of-the-art methods [6], [9], [13].

Regarding the representation of unstructured and unordered 3D LiDAR points, there are two common approaches as depicted in Fig. 1: point-wise representation and projection-based rendering. We refer the interested readers to [8] for more details on the 3D data representation.

Point-wise methods [14], [15] directly process the raw irregular 3D points without applying any additional transformation or pre-processing. Shared multi-layer perceptron-based PointNet [14], the subsequent work PointNet++ [15], and *superpoint* graph SPG networks [16] are considered in this group. Although such methods are powerful on small point clouds, their processing capacity and memory requirement unfortunately become inefficient when it comes to large LiDAR point sets. To accelerate point-wise operations, additional cues, e.g. from camera images, are employed as successfully introduced in [17].

Projection-based methods rather transform the 3D point cloud into various formats such as voxel cells [12], [18], [19], multi-view representation [20], lattice structure [21], [22], and rasterized images [1], [6], [9]. In the multi-view representation, a 3D point cloud is projected onto multiple 2D surfaces from various virtual camera viewpoints. Each view is then processed by a multi-stream network as in [20]. In the lattice structure, the raw unorganized point cloud is interpolated to a permutohedral sparse lattice where bilateral convolutions are applied to occupied lattice sectors only [21]. Methods relying on the voxel representation discretize the 3D space into 3D volumetric space (i.e. voxels) and assign each point to the corresponding voxel [12], [18], [19]. Sparsity and irregularity in point clouds, however, yield redundant

computations in voxelized data since many voxel cells may stay empty. A common attempt to overcome the sparsity in LiDAR data is to project 3D point clouds into 2D image space either in the top-down Bird-Eye-View [1], [23], [24] or spherical Range-View (RV) (i.e. panoramic view) [7], [6], [9], [10] formats. Unlike point-wise and other projection-based approaches, such 2D rendered image representations are more compact, dense and computationally cheaper as they can be processed by standard 2D convolutional layers. Therefore, our *SalsaNext* model initially projects the LiDAR point cloud into 2D RV image generated by mapping each 3D point onto a spherical surface.

Note that in this study we focus on semantic segmentation of LiDAR-only data and thus ignore multi-model approaches that fuse, e.g. LiDAR and camera data as in [17].

III. METHOD

In this section, we give a detailed description of our method starting with the point cloud representation. We then continue with the network architecture, loss function, and training details.

A. LiDAR Point Cloud Representation

As in [7], we project the unstructured 3D LiDAR point cloud onto a spherical surface to generate the LiDAR's native Range View (RV) image. This process leads to dense and compact point cloud representation which allows standard convolution operations.

In the 2D RV image, each raw LiDAR point (x, y, z) is mapped to an image coordinate (u, v) as

$$\begin{pmatrix} u \\ v \end{pmatrix} = \begin{pmatrix} \frac{1}{2}[1 - \arctan(y, x)\pi^{-1}]w \\ [1 - (\arcsin(z, r^{-1}) + f_{down})f^{-1}]h \end{pmatrix},$$

where h and w denote the height and width of the projected image, r represents the range of each point as $r = \sqrt{x^2 + y^2 + z^2}$ and f defines the sensor vertical field of view as $f = |f_{down}| + |f_{up}|$.

Following the work of [7], we considered the full 360° field-of-view in the projection process. During the projection, 3D point coordinates (x, y, z) , the intensity value (i) and the range index (r) are stored as separate RV image channels. This yields a $[w \times h \times 5]$ image to be fed to the network.

B. Network Architecture

The architecture of the proposed *SalsaNext* is illustrated in Fig. 2. The input to the network is an RV image projection of the point cloud as described in section III-A.

SalsaNext is built upon the base *SalsaNet* model [1] which follows the standard encoder-decoder architecture with a bottleneck compression rate of 16. The original *SalsaNet* encoder contains a series of ResNet blocks [25] each of which is followed by dropout and downsampling using a strided convolution or pooling. The decoder blocks apply transpose convolutions and fuse upsampled features with that of the early residual blocks via skip connections. To further exploit descriptive spatial cues, a stack of convolution is inserted after the skip connection. Shaded gray box in Fig. 2 depicts the original *SalsaNet* structure.

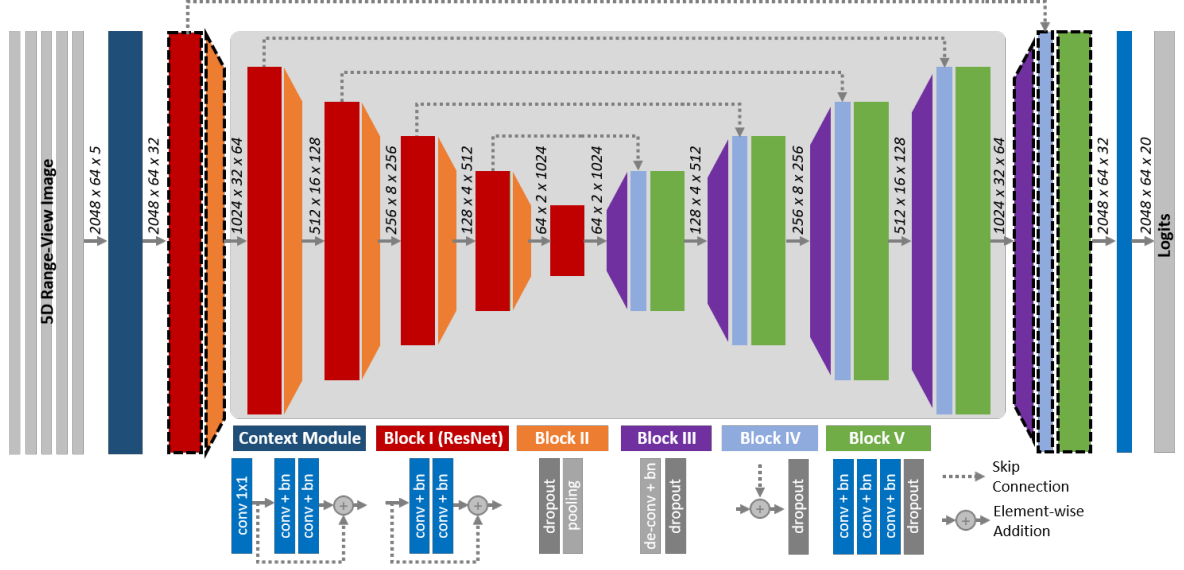


Fig. 2. Architecture of the proposed *SalsaNext* model. Shaded gray box, except the attention blocks, indicates the original *SalsaNet* model. Encoder part is composed of a series of ResNet blocks. Decoder part rather upsamples feature maps and then fuses them with the respective early residual block responses via skip connections. Convolution layers in Blocks I-V and context module are combined with the leaky-ReLU activation functions and batch normalization (bn) layers. Blocks with dashed edges indicate those that do not employ the dropout.

As illustrated in Fig. 2, we in this study improved the base structure of *SalsaNet* in the following manner:

Extra Layer: To more efficiently process high-resolution point cloud projections, we increased the depth of *SalsaNet* by adding one extra layer in the encoder and one in the decoder. These new layers also increased the compression factor of the bottleneck from 16 to 32.

Contextual Module: One of the main issues with the semantic segmentation is the lack of contextual information throughout the network. The global context information gathered by larger receptive fields plays a crucial role in learning complex correlations between classes [5]. To aggregate the context information in different regions, we fuse a larger receptive field with a smaller one by adding 3×3 and 1×1 kernels right at the beginning of the network. This helps us capture the global context alongside with more detailed spatial information.

Central Encoder-Decoder Dropout: As shown by quantitative experiments in [4], inserting dropout only to the central encoder and decoder layers results in better segmentation performance. It is because the lower network layers extract basic features such as edges and corners [26] which are consistent over the data distribution and dropping out these layers will prevent the network to properly form the higher level features in the deeper layers. This eventually leads to poor network performance. We, therefore, insert dropout in every encoder-decoder layer except the first and last one which are highlighted by dashed edges in Fig. 2.

Average Pooling: In the base *SalsaNet* model the down-sampling was performed via a strided convolution which introduces additional learning parameters. Given that the down-sampling process is relatively straightforward, we hypothesize that learning at this level would not be needed.

Thus, to allocate less memory *SalsaNext* switches to average pooling for the downsampling.

All these updates form the proposed *SalsaNext* network. Furthermore, we applied a 1×1 convolution after the decoder unit to make the channel numbers the same with the total number of semantic classes. The final feature map is finally passed to a soft-max classifier to compute pixel-wise classification scores. Note that each convolution layer in the *SalsaNext* model employs a leaky-ReLU activation function and is followed by batch normalization to solve the internal covariant shift. Dropout is then placed after the batch normalization. It can, otherwise, result in a shift in the weight distribution which can minimize the batch normalization effect during training as shown in [27].

C. Loss Function

Datasets with imbalanced classes introduce a challenge for neural networks. Take an example of a bicycle or traffic sign which appears much less compared to the vehicles in the autonomous driving scenarios. This makes the network more biased towards to the classes that emerge more in the training data and thus yields significantly poor network performance.

To cope with the imbalanced class problem, we follow the same strategy in *SalsaNet* and add more value to the under-represented classes by weighting the softmax cross-entropy loss \mathcal{L}_{wce} with the inverse square root of class frequency as

$$\mathcal{L}_{wce}(y, \hat{y}) = - \sum_i \alpha_i p(y_i) \log(p(\hat{y}_i)) \quad \text{with} \quad \alpha_i = 1/\sqrt{f_i},$$

where y_i and \hat{y}_i define the true and predicted class labels and f_i stands for the frequency, i.e. the number of points, of the i^{th} class. This reinforces the network response to the classes appearing less in the dataset.

In contrast to *SalsaNet*, we here also incorporate the *Lovász-Softmax* loss [2] in the learning procedure to maxi-

mize the intersection-over-union (IoU) score, i.e. the Jaccard index. The IoU metric (see section IV-A) is the most commonly used metric to evaluate the segmentation performance. Nevertheless, IoU is a discrete and not derivable metric that does not have a direct way to be employed as a loss. In [2], the authors adopt this metric with the help of the Lovász extension for submodular functions. Considering the IoU as a hypercube where each vertex is a possible combination of the class labels, we relax the IoU score to be defined everywhere inside of the hypercube. In this respect, the *Lovász-Softmax* loss (\mathcal{L}_{ls}) can be formulated as follows:

$$\mathcal{L}_{ls} = \frac{1}{|C|} \sum_{c \in C} \overline{\Delta_{J_c}}(m(c)), \text{ and } m_i(c) = \begin{cases} 1 - x_i(c) & \text{if } c = y_i(c) \\ x_i(c) & \text{otherwise} \end{cases},$$

where $|C|$ represents the class number, $\overline{\Delta_{J_c}}$ defines the Lovász extension of the Jaccard index, $x_i(c) \in [0, 1]$ and $y_i(c) \in \{-1, 1\}$ hold the predicted probability and ground truth label of pixel i for class c , respectively.

Finally, the total loss function of *SalsaNext* is a linear combination of both weighted cross-entropy, *Lovász-Softmax* losses, regularization and *aleatoric* loss as follows $\mathcal{L} = \mathcal{L}_{wce} + \mathcal{L}_{ls}$.

D. Optimizer And Regularization

As an optimizer, we employed stochastic gradient descent with an initial learning rate of 0.05 which is decayed by 0.01 after each epoch. We also applied an L2 penalty with $\lambda = 0.0001$ and a momentum of 0.9. The batch size and spatial dropout probability were fixed at 30 and 0.2, respectively.

E. Post-processing

The main drawback of the projection-based point cloud representation is the information loss due to discretization errors and blurry convolutional layer responses. This problem emerges when, for instance, the RV image is re-projected back to the original 3D space. The reason is that during the image rendering process, multiple LiDAR points may get assigned to the very same image pixel which leads to misclassification of, in particular, the object edges. This effect becomes more obvious, for instance, when the objects cast a shadow in the background scene.

To cope with these back-projection related issues, we employ the kNN-based post-processing technique introduced in [7]. The post-processing is applied to every LiDAR point by using a window around each corresponding image pixel, that will be translated into a subset of point clouds. Next, a set of closest neighbors is selected with the help of kNN. The assumption behind using the range instead of the Euclidian distances lies in the fact that a small window is applied, making the range of close (u, v) points serve as a good proxy for the Euclidian distance in the three-dimensional space. For more details, we refer the readers to [7].

Note that this post-processing is applied to the network output during inference only and has no effect on learning.

IV. EXPERIMENTS

We evaluate the performance of *SalsaNext* and compare with the other state-of-the-art semantic segmentation methods on the large-scale challenging Semantic-KITTI dataset [3] which provides over 43K point-wise annotated full 3D LiDAR scans. We follow exactly the same protocol in [7] and divide the dataset into training, validation, and test splits. Over 21K scans (sequences between 00 and 10) are used for training, where scans from sequence 08 are particularly dedicated to validation. The remaining scans (between sequences 11 and 21) are used as test split. The dataset has in total 22 classes 19 of which are evaluated on the test set by the official online benchmark platform. We implement our model in PyTorch and release the code for public use <https://github.com/TiagoCortinhal/SalsaNext>

A. Evaluation Metric

To evaluate the results of our model we use the Jaccard Index, also known as mean intersection-over-union (IoU) over all classes that is given by:

$$mIoU = \frac{1}{C} \sum_{i=1}^C \frac{|\mathcal{P}_i \cap \mathcal{G}_i|}{|\mathcal{P}_i \cup \mathcal{G}_i|}$$

Where \mathcal{P}_i is the set of point with a class prediction i , \mathcal{G}_i the labelled set for class i and $||$ the cardinality of the set.

B. Quantitative Results

Obtained quantitative results compared to other point-wise and projection-based approaches are reported in Table I. Our proposed model *SalsaNext* considerably outperforms the others by leading to the highest mean IoU score (54.5%) which is +2.3% over the previous state-of-the-art methods [7], [22]. In contrast to the original *SalsaNet*, we also obtain more than 10% improvement on the accuracy. When it comes to the performance of each individual category, *SalsaNext* performs better in 9 categories out of 19. Note that in some of these remaining 10 categories (e.g. road, sidewalk, other-ground, and fence) *SalsaNext* still has a comparable performance with the other approaches.

C. Qualitative Results

For the qualitative evaluation, Fig. 3 shows some sample semantic segmentation results generated by *SalsaNext* on the Semantic-KITTI test set. In this figure, only for visualization purpose, segmented object points are also projected back to the respective camera image. We, here, emphasize that these camera images have not been used for training of *SalsaNext*. As depicted in Fig. 3, *SalsaNext* can, to a great extent, distinguish road, car, and other object points. In the supplementary video¹, we provide more qualitative results.

¹<https://youtu.be/WEAaq7GWSz0>

	Approach	Size	car	bicycle	motorcycle	truck	other-vehicle	person	bicyclist	motorcyclist	road	parking	sidewalk	other-ground	building	fence	vegetation	trunk	terrain	pole	traffic-sign	mean-IoU
Point-wise	Pointnet [14]	50K pts	46.3	1.3	0.3	0.1	0.8	0.2	0.2	0.0	61.6	15.8	35.7	1.4	41.4	12.9	31.0	4.6	17.6	2.4	3.7	14.6
	Pointnet++ [15]		53.7	1.9	0.2	0.9	0.2	0.9	1.0	0.0	72.0	18.7	41.8	5.6	62.3	16.9	46.5	13.8	30.0	6.0	8.9	20.1
	SPGraph [16]		68.3	0.9	4.5	0.9	0.8	1.0	6.0	0.0	49.5	1.7	24.2	0.3	68.2	22.5	59.2	27.2	17.0	18.3	10.5	20.0
	SPLATNet [21]		66.6	0.0	0.0	0.0	0.0	0.0	0.0	0.0	70.4	0.8	41.5	0.0	68.7	27.8	72.3	35.9	35.8	13.8	0.0	22.8
	TangentConv [28]		86.8	1.3	12.7	11.6	10.2	17.1	20.2	0.5	82.9	15.2	61.7	9.0	82.8	44.2	75.5	42.5	55.5	30.2	22.2	35.9
	RandLa-Net [29]		94.0	19.8	21.4	42.7	38.7	47.5	48.8	4.6	90.4	56.9	67.9	15.5	81.1	49.7	78.3	60.3	59.0	44.2	38.1	50.3
Projection-based	SqueezeSeg [6]	64×2048 pixels	68.8	16.0	4.1	3.3	3.6	12.9	13.1	0.9	85.4	26.9	54.3	4.5	57.4	29.0	60.0	24.3	53.7	17.5	24.5	29.5
	SqueezeSeg-CRF [6]		68.3	18.1	5.1	4.1	4.8	16.5	17.3	1.2	84.9	28.4	54.7	4.6	61.5	29.2	59.6	25.5	54.7	11.2	36.3	30.8
	SqueezeSegV2 [9]		81.8	18.5	17.9	13.4	14.0	20.1	25.1	3.9	88.6	45.8	67.6	17.7	73.7	41.1	71.8	35.8	60.2	20.2	36.3	39.7
	SqueezeSegV2-CRF [9]		82.7	21.0	22.6	14.5	15.9	20.2	24.3	2.9	88.5	42.4	65.5	18.7	73.8	41.0	68.5	36.9	58.9	12.9	41.0	39.6
	RangeNet21 [7]		85.4	26.2	26.5	18.6	15.6	31.8	33.6	4.0	91.4	57.0	74.0	26.4	81.9	52.3	77.6	48.4	63.6	36.0	50.0	47.4
	RangeNet53 [7]		86.4	24.5	32.7	25.5	22.6	36.2	33.6	4.7	91.8	64.8	74.6	27.9	84.1	55.0	78.3	50.1	64.0	38.9	52.2	49.9
	RangeNet53++ [7]		91.4	25.7	34.4	25.7	23.0	38.3	38.8	4.8	91.8	65.0	75.2	27.8	87.4	58.6	80.5	55.1	64.6	47.9	55.9	52.2
	LatticeNet [22]		88.6	12.0	20.8	43.3	24.8	34.2	39.9	60.9	88.8	64.6	73.8	25.6	86.9	55.2	76.4	57.9	54.7	41.5	42.7	52.2
	SalsaNet [1]	64×2048 pixels	83.3	25.4	23.9	23.9	17.3	32.5	30.4	8.3	89.7	51.6	70.4	19.9	80.2	45.9	71.5	38.1	61.2	26.9	39.4	44.2
	SalsaNext [Ours]	64×2048 pixels	90.9	36.4	29.5	21.7	19.9	52.0	52.7	16.0	90.9	58.1	74.0	27.8	87.9	58.2	81.8	61.7	66.3	51.7	58.0	54.5

TABLE I

QUANTITATIVE COMPARISON ON SEMANTIC-KITTI TEST SET (SEQUENCES 11 TO 21). IOU SCORES ARE GIVEN IN PERCENTAGE (%).

D. Ablation Study

In this ablative analysis, we investigate the individual contribution of each improvements over the original *SalsaNet* model. Table II shows the total number of model parameters together with the obtained mIoU scores on the Semantic-KITTI test set before and after applying the kNN-based post processing step (see section III-E).

As depicted in table II, each operation on *SalsaNet* has a unique improvement on the accuracy. The post processing step leads to certain jump in the accuracy. The highest jump in the model parameters is observed when the new layers are inserted. We can achieve the highest accuracy score of 54.5% by having almost 50% less model parameters (i.e. 23.26M) in contrast to RangeNet++ [7] which has 50M parameters. Overall improvement on the original *SalsaNet* model is more than 10% (54.5% versus 44.2%).

	mean IoU (w/o kNN)	mean IoU (+kNN)	Number of Parameters
SalsaNet [1]	44.2	45.4	6.58M
+ extra layers	45.2	46.6	26.38M
+ context module	46.4	48.2	26.40M
+ new dropout	49.6	52.0	26.40M
+ average pooling	50.4	52.9	23.26M
+ Lovász-Softmax loss	51.5	54.5	23.26M

TABLE II
ABLATIVE ANALYSIS.

E. Runtime Evaluation

Runtime performance is crucial in autonomous driving. Table III shows the single forward pass runtime performance of *SalsaNext* in comparison to the other networks. For a fair comparison, we measure the inference time of all scans in a sample test scenario (sequence 13) using the same NVIDIA Quadro P6000-24GB GPU card. Obtained mean runtime



Fig. 3. Sample qualitative results showing successes of our proposed *SalsaNext* method on the Semantic-KITTI test set (test sequence 13) [best view in color]. At the bottom of each scene, the range-view image of the network response is shown. Camera images on the top left show the projected segments. Note that the corresponding camera images are only for visualization purposes and have not been used in the training.

	Mean (msec)	Std (msec)	Speed (fps)
RangeNet++ [7]	14.27	2.86	70 Hz
SalsaNet [1]	10.38	1.72	96 Hz
SalsaNext [Ours]	12.00	1.99	83 Hz

TABLE III

RUNTIME PERFORMANCE ON THE SEMANTIC-KITTI DATASET [3]

values and standard deviations are reported in Table III. The proposed *SalsaNext* clearly exhibits better performance compared to the RangeNet++ [7] and has a comparable performance with the original *SalsaNet* model. Note also that the standard deviation of the *SalsaNext* runtime is also relatively less than the RangeNet++ [7], which plays a crucial role in the stability of the self-driving perception modules. Recall also Fig. 1 which shows the overall runtime versus accuracy plot for the state-of-the-art methods and *SalsaNext*.

Consequently, our proposed *SalsaNext* network inference (a single forward pass) time can reach up to 83 Hz while providing the highest accuracy 54.5%. We here emphasize that this achieved high speed is significantly faster than the sampling rate of mainstream LiDAR scanners which typically work at 10Hz.

V. CONCLUSION

In this work, we presented our improved semantic segmentation network, named *SalsaNext*, that can process the full 360° LiDAR scan in real-time. *SalsaNext* builds up on the *SalsaNet* model and can already achieve over 10% more accuracy. In contrast to other state-of-the-art methods, *SalsaNext* returns +2.3% better mIoU score. We plan to use *SalsaNext* to bootstrap the detection and tracking processes as a future task.

REFERENCES

- [1] E. E. Aksoy, S. Baci, and S. Cavdar, "Salsanet: Fast road and vehicle segmentation in lidar point clouds for autonomous driving," *CoRR*, 2019. [Online]. Available: <http://arxiv.org/abs/1909.08291>
- [2] M. Berman, A. Rannen Triki, and M. B. Blaschko, "The lovasz-softmax loss: A tractable surrogate for the optimization of the intersection-over-union measure in neural networks," in *CVPR*, 2018, pp. 4413–4421.
- [3] J. Behley, M. Garbade, A. Milioto, J. Quenzel, S. Behnke, C. Stachniss, and J. Gall, "SemanticKITTI: A Dataset for Semantic Scene Understanding of LiDAR Sequences," in *ICCV*, 2019.
- [4] A. Kendall, V. Badrinarayanan, and R. Cipolla, "Bayesian segnet: Model uncertainty in deep convolutional encoder-decoder architectures for scene understanding," *arXiv preprint arXiv:1511.02680*, 2015.
- [5] R. P. K. Poudel, S. Liwicki, and R. Cipolla, "Fast-scnn: Fast semantic segmentation network," *CoRR*, vol. abs/1902.04502, 2019. [Online]. Available: <http://arxiv.org/abs/1902.04502>
- [6] B. Wu, A. Wan, X. Yue, and K. Keutzer, "Squeezeseg: Convolutional neural nets with recurrent crf for real-time road-object segmentation from 3d lidar point cloud," *ICRA*, 2018.
- [7] A. Milioto, I. Vizzo, J. Behley, and C. Stachniss, "RangeNet++: Fast and Accurate LiDAR Semantic Segmentation," in *IROS*, 2019.
- [8] Y. Guo, H. Wang, Q. Hu, H. Liu, L. Liu, and M. Bennamoun, "Deep learning for 3d point clouds: A survey," *CoRR*, 2019. [Online]. Available: <https://arxiv.org/abs/1912.12033>
- [9] B. Wu, X. Zhou, S. Zhao, X. Yue, and K. Keutzer, "Squeezesegv2: Improved model structure and unsupervised domain adaptation for road-object segmentation from a lidar point cloud," in *ICRA*, 2019.
- [10] Y. Wang, T. Shi, P. Yun, L. Tai, and M. Liu, "Pointseg: Real-time semantic segmentation based on 3d lidar point cloud," *CoRR*, vol. abs/1807.06288, 2018.
- [11] E. Shelhamer, J. Long, and T. Darrell, "Fully convolutional networks for semantic segmentation," *PAMI*, 2016.
- [12] C. Zhang, W. Luo, and R. Urtasun, "Efficient convolutions for real-time semantic segmentation of 3d point clouds," in *Proceedings of the International Conference on 3D Vision (3DV)*, 2018.
- [13] O. Ronneberger, P. Fischer, and T. Brox, "U-net: Convolutional networks for biomedical image segmentation," in *Medical Image Computing and Computer-Assisted Intervention*, 2015, pp. 234–241.
- [14] C. R. Qi, H. Su, K. Mo, and L. J. Guibas, "Pointnet: Deep learning on point sets for 3d classification and segmentation," in *IEEE Conf. on Computer Vision and Pattern Recognition (CVPR)*, 2017.
- [15] C. R. Qi, L. Yi, H. Su, and L. J. Guibas, "Pointnet++: Deep hierarchical feature learning on point sets in a metric space," in *In Proc. of the Advances in Neural Information Processing Systems (NIPS)*, 2017.
- [16] L. Landrieu and M. Simonovsky, "Large-scale point cloud semantic segmentation with superpoint graphs," in *CVPR*, 2018.
- [17] C. R. Qi, W. Liu, C. Wu, H. Su, and L. J. Guibas, "Frustum pointnets for 3d object detection from RGB-D data," *CoRR*, 2017. [Online]. Available: <http://arxiv.org/abs/1711.08488>
- [18] Y. Zhou and O. Tuzel, "Voxelnet: End-to-end learning for point cloud based 3d object detection," in *2018 IEEE/CVF Conference on Computer Vision and Pattern Recognition*, June 2018, pp. 4490–4499.
- [19] L. P. Tchammi, C. B. Choy, I. Armeni, J. Gwak, and S. Savarese, "Segcloud: Semantic segmentation of 3d point clouds," in *IEEE Intl. Conf. on 3D Vision (3DV)*, 2017, p. 537547.
- [20] F. J. Lawin, M. Danelljan, P. Tosteberg, G. Bhat, F. S. Khan, and M. Felsberg, "Deep projective 3d semantic segmentation," *CoRR*, 2017. [Online]. Available: <http://arxiv.org/abs/1705.03428>
- [21] H. Su, V. Jampani, D. Sun, S. Maji, E. Kalogerakis, M. Yang, and J. Kautz, "Splatnet: Sparse lattice networks for point cloud processing," in *CVPR*, 2018.
- [22] R. A. Rosu, P. Schtt, J. Quenzel, and S. Behnke, "Latticenet: Fast point cloud segmentation using permutohedral lattices," 2019.
- [23] Y. Zeng, Y. Hu, S. Liu, J. Ye, Y. Han, X. Li, and N. Sun, "Rt3d: Real-time 3-d vehicle detection in lidar point cloud for autonomous driving," *IEEE RAL*, vol. 3, no. 4, pp. 3434–3440, Oct 2018.
- [24] M. Simon, S. Milz, K. Amende, and H. Gross, "Complex-yolo: Real-time 3d object detection on point clouds," *CoRR*, 2018.
- [25] K. He, X. Zhang, S. Ren, and J. Sun, "Deep residual learning for image recognition," in *Proceedings of the IEEE conference on computer vision and pattern recognition*, 2016, pp. 770–778.
- [26] M. D. Zeiler and R. Fergus, "Visualizing and understanding convolutional networks," *CoRR*, vol. abs/1311.2901, 2013. [Online]. Available: <http://arxiv.org/abs/1311.2901>
- [27] X. Li, S. Chen, X. Hu, and J. Yang, "Understanding the disharmony between dropout and batch normalization by variance shift," *arXiv preprint arXiv:1801.05134*, 2018.
- [28] M. Tatarchenko, J. Park, V. Koltun, and Q. Zhou, "Tangent convolutions for dense prediction in 3d," in *CVPR*, 2018.
- [29] Q. Hu, B. Yang, L. Xie, S. Rosa, Y. Guo, Z. Wang, N. Trigoni, and A. Markham, "Randla-net: Efficient semantic segmentation of large-scale point clouds," 2019.